4-2014

Simulations of inner magnetosphere dynamics with an expanded RAM-SCB model and comparisons with Van Allen Probes observations

Vania K. Jordanova
Los Alamos National Laboratory

Y. Yu
Los Alamos National Laboratory

J. T. Niehof
Los Alamos National Laboratory

R. M. Skoug
Los Alamos National Laboratory

Geoffrey Reeves
Los Alamos National Laboratory

See next page for additional authors

Recommended Citation

Jordanova, V. K., Y. Yu, J. T. Niehof, R. M. Skoug, G. D. Reeves, C. A. Kletzing, J. F. Fennell, and H. E. Spence (2014), Simulations of inner magne-tosphere dynamics with an expanded RAM-SCB model and comparisons with Van Allen Probes observations, Geophys. Res. Lett., 41, 2687–2694, doi:10.1002/2014GL059533

AGU PUBLICATIONS

Geophysical Research Letters

RESEARCH LETTER
10.1002/2014GL059533

Key Points:
- Expanded RAM-SCB model reproduces well high-energy (>50 keV) MagEIS observations
- The magnetic field is depressed as close as ~4.5 R_E during even a moderate storm
- EMIC wave growth extends on duskside from ~6 to ~9 R_E during storm main phase

Correspondence to:
V. K. Jordanova,
vania@lanl.gov

Citation:
Jordanova, V. K., Y. Yu, J. T. Niehof, R. M. Skoug, G. D. Reeves, C. A. Kletzing, J. F. Fennell, and H. E. Spence (2014), Simulations of inner magnetosphere dynamics with an expanded RAM-SCB model and comparisons with Van Allen Probes observations, *Geophys. Res. Lett.*, *41*, 2687–2694, doi:10.1002/2014GL059533.

Received 5 FEB 2014
Accepted 27 MAR 2014
Accepted article online 2 APR 2014
Published online 16 APR 2014

Simulations of inner magnetosphere dynamics with an expanded RAM-SCB model and comparisons with Van Allen Probes observations

V. K. Jordanova[1], Y. Yu[1], J. T. Niehof[1], R. M. Skoug[1], G. D. Reeves[1], C. A. Kletzing[2], J. F. Fennell[3], and H. E. Spence[4]

[1]Space Science and Applications, Los Alamos National Laboratory, Los Alamos, New Mexico, USA, [2]Department of Physics and Astronomy, University of Iowa, Iowa City, Iowa, USA, [3]Aerospace Corporation, Los Angeles, California, USA, [4]Institute for the Study of Earth, Oceans, and Space, University of New Hampshire, Durham, New Hampshire, USA

Abstract Simulations from our newly expanded ring current-atmosphere interactions model with self-consistent magnetic field (RAM-SCB), now valid out to 9 R_E, are compared for the first time with Van Allen Probes observations. The expanded model reproduces the storm time ring current buildup due to the increased convection and inflow of plasma from the magnetotail. It matches Magnetic Electron Ion Spectrometer (MagEIS) observations of the trapped high-energy (>50 keV) ion flux; however, it underestimates the low-energy (<10 keV) Helium, Oxygen, Proton, and Electron (HOPE) observations. The dispersed injections of ring current ions observed with the Energetic particle, Composition, and Thermal plasma (ECT) suite at high (>20 keV) energy are better reproduced using a high-resolution convection model. In agreement with Electric and Magnetic Field Instrument Suite and Integrated Science (EMFISIS) observations, RAM-SCB indicates that the large-scale magnetic field is depressed as close as ~4.5 R_E during even a moderate storm. Regions of electromagnetic ion cyclotron instability are predicted on the duskside from ~6 to ~9 R_E, indicating that previous studies confined to geosynchronous orbit may have underestimated their scattering effect on the energetic particles.

1. Introduction

Numerical models are important tools to enhance our understanding and ability to predict highly dynamic and coupled space systems such as Earth's magnetosphere. During active conditions, the solar wind and the ionosphere provide rich sources of plasma to the geomagnetic tail [*Chappell et al.*, 1987]. Plasma sheet particles are transported earthward, energized, and trapped by the magnetic field of the Earth to form the ring current, whose electron component represents a seed population for the radiation belts [e.g., *Jordanova*, 2012]. The anisotropic ring current ion and electron distributions generate diverse wave modes (electromagnetic ion cyclotron (EMIC), whistler, and magnetosonic), which may cause further particle acceleration and loss through energy and pitch angle scattering [e.g., *Summers et al.*, 1998; *Thorne et al.*, 2006]. An outstanding question is to determine the temporal evolution and spatial extent of these waves during geomagnetic storms in order to quantify their role in (1) the acceleration of particles forming the hazardous radiation belts and (2) particle precipitation and loss to the atmosphere. Major computational challenges are to develop models that couple self-consistently the plasma and the fields across various regions of the magnetosphere and which include both large-scale and microscale physics.

The majority of the plasma pressure in the Earth's inner magnetosphere is carried by ring current ions in the energy range ~1–200 keV [*Daglis et al.*, 1993]. The westward drifting high-energy ions, and eastward drifting electrons, generate a ring current which intensifies significantly as the geomagnetic activity increases [*Le et al.*, 2004]. The spatial and temporal development of the ring current considerably affects the magnetic field topology in the inner magnetosphere. During the storm main phase when the convection is strong and the ring current particles penetrate close to Earth, the intensified westward ring current weakens the magnetic field especially across the nightside. The distorted magnetic field modifies the ion and electron trajectories in the near-Earth region, leading to adiabatic redistribution and nonadiabatic losses of the energetic particles [*Kim and Chan*, 1997]. To differentiate between real (nonadiabatic) loss and changes due to adiabatic motion, knowledge of the magnetic field over the entire drift orbit of the particle is needed; this can be

provided by numerical models that specify the magnetic field on a global scale. Previous research efforts have led to the development of empirical magnetic field models [e.g., *Tsyganenko*, 1989], global MHD models [e.g., *Powell et al.*, 1999], or inner magnetosphere models [e.g., *Lemon et al.*, 2004; *Zaharia et al.*, 2006].

The recent launch of the Van Allen Probes (formerly known as the Radiation Belt Storm Probes, RBSP) mission [*Mauk et al.*, 2012] provides an excellent opportunity for further validation of models that simulate the dynamics of the inner magnetosphere. This mission was launched on 30 August 2012 into a near-equatorial, elliptical orbit around Earth with apogee at ~6 R_E, with a complement of unprecedented high-resolution instruments to provide the best possible quality measurements in the inner magnetosphere. Its primary goal is to identify dominant mechanisms for the transport, acceleration, and loss of radiation belt particles which, as explained above, is intrinsically related to understanding ring current dynamics. This study investigates the injection and trapping of ring current ions, as well as the distortion of the large-scale magnetic field, during a moderate storm with $Dst \approx -60$ nT that occurred on 1 November 2012. Simulation results from our magnetically self-consistent model [e.g., *Jordanova et al.*, 2010] newly expanded to 9 R_E and driven for the first time by the *Weimer* [2005] electric field model and a plasma sheet source model from *Tsyganenko and Mukai* [2003] are compared with in situ observations from the Van Allen Probes. The generation of EMIC waves and the possible consequences for energetic particle precipitation and radiation belt dynamics are also discussed.

2. Data-Model Comparisons

We present first results from our ring current model with self-consistent magnetic field (RAM-SCB), where its outer boundary is expanded from 6.5 to 9 R_E. The RAM-SCB model includes alternating steps between two modules: (1) the ring current-atmosphere interactions model (RAM), which simulates the spatial and temporal evolution of ring current H^+, O^+, and He^+ ions and electrons in dynamic electric and magnetic fields [*Jordanova et al.*, 1998, 2010] and (2) a three-dimensional (3-D) Euler potential-based plasma equilibrium code (SCB) [*Zaharia et al.*, 2006], which calculates the magnetic field in force balance with the plasma pressure from the ring current particles. The expanded model includes all magnetic local times (MLT), inner boundary at radial distance $R_o = 2\ R_E$, energies from ~1 keV to 400 keV, and pitch angles from 0° to 90°. As the RAM-SCB outer boundary is moved from 6.5 to 9 R_E, in this first study we specify the plasma boundary conditions after the empirical TM03 [*Tsyganenko and Mukai*, 2003] plasma sheet model based on Geotail data, and the magnetic field boundary conditions after the *Kp*-dependent empirical model of *Tsyganenko* [1989]. Another development of RAM-SCB is its coupling with the improved electric field model of *Weimer* [2005] which has more accurate field values and a better reproduction of nonlinear saturation effects in the solar wind-magnetosphere coupling.

We investigate the dynamics of the ring current during the moderate storm of 1 November 2012, one of the first storms observed by the Van Allen Probes. Figure 1 shows the interplanetary observations and geomagnetic indices during the investigated period, taken from the OMNIWeb 5 min database. An interplanetary shock is observed at ~15:30 UT 31 October followed by an increase of solar wind density and solar wind speed (Figures 1a–1b). The north-south component of the interplanetary magnetic field (IMF) is fluctuating around $B_z = 0$ until ~02:00 UT 1 November when it begins a southward excursion to about −12 nT at ~10:00 UT, followed by a northward rotation thereafter. These interplanetary conditions triggered a moderate geomagnetic storm with minima $Dst \approx -60$ nT at 14:00 UT and 21:00 UT and maximum $Kp = 5^-$ at 16:00 UT (not shown). The minimum $AL \approx -1500$ nT was reached at ~15:00 UT, when the polar cap index based on data from Thule station near the North Pole [*Troshichev et al.*, 1988] reached maximum $PCN \approx 5$. The cross polar cap potential (CPCP) drop obtained with the W05 [*Weimer*, 2005] ionospheric electric potential remained elevated between ~08:00 UT and 14:00 UT with a peak of ~85 kV at ~10:00 UT, while the CPCP drop from the *Kp*-dependent V-S model [*Volland*, 1973; *Stern*, 1975] had a peak of ~75 kV at 16:30 UT.

The plasma sheet ion density and temperature calculated with the TM03 empirical model [*Tsyganenko and Mukai*, 2003] are plotted in Figures 1c and 1d, respectively. This statistical model is based on particle data taken by Geotail spacecraft between 1994 and 1998 and concurrent solar wind and IMF data provided by Wind and IMP 8 spacecraft. The ion density is mostly controlled by the solar wind proton density and therefore increases abruptly at ~16:00 UT on 31 October. The ion temperature is controlled both by the solar wind speed and the IMF B_z, and it reaches maximum at ~12:00 UT on 1 November. The similarity between

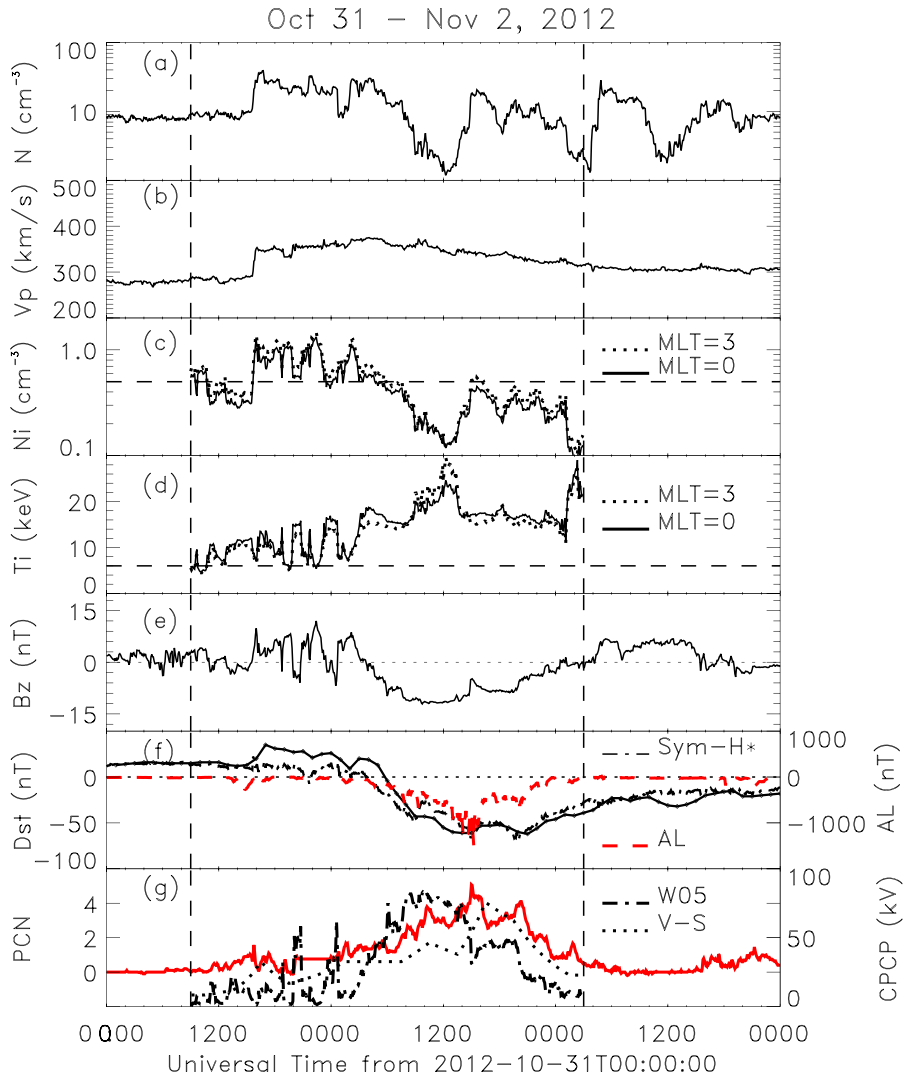

Figure 1. Interplanetary and magnetospheric data during 31 October to 2 November 2012. (a) Solar wind proton density, (b) solar wind speed, (c) TM03 plasma sheet ion density, (d) TM03 plasma sheet ion temperature, and (e) the B_z (GSM) component of the magnetic field. (f) The measured *Dst* (solid line), *AL* (dashed line), and pressure-corrected *SYM-H* (dash-dotted line) indices. (g) The *PCN* index (solid line), and the W05 (dash-dotted line) and V-S (dotted line) cross polar cap potential drop. The RAM-SCB simulation is run for the time period indicated with vertical dashed lines in Figures 1a–1g.

the model results at MLT = 0 (solid line) and MLT = 3 (dotted) indicates that there is no significant azimuthal asymmetry in the TM03 model. These data are used to set up the boundary conditions of RAM-SCB at 9 R_E during the investigated period indicated with vertical dashed lines in Figure 1.

We start the RAM-SCB simulation at quiet time (09:00 UT 31 October) specifying the ring current H^+, O^+, and He^+ initial conditions after measurements from the Helium, Oxygen, Proton, and Electron (HOPE) mass spectrometer [*Funsten et al.*, 2013] and the Magnetic Electron Ion Spectrometer (MagEIS) [*Blake et al.*, 2013], both of which are part of the Energetic particle, Composition, and Thermal plasma (ECT) suite [*Spence et al.*, 2013] on the Van Allen Probes. This NASA mission consists of two Sun-pointing, spin-stabilized spacecraft (RBSP-A and RBSP-B) with a nominal spin period of ~11 s equipped with identical instrumentation. During the investigated period the HOPE instrument measured the charged particles, with composition information, from ~20 eV to 50 keV, while the MagEIS spectrometer provided total ion measurements over the energy range ~50 keV to 1 MeV. To set up the initial conditions we use spin-averaged differential fluxes obtained as a function of radial distance from Earth during the prestorm satellite orbit, assuming azimuthal symmetry (a reasonable approximation for the high-energy population on closed drift paths) and isotropy in pitch angle.

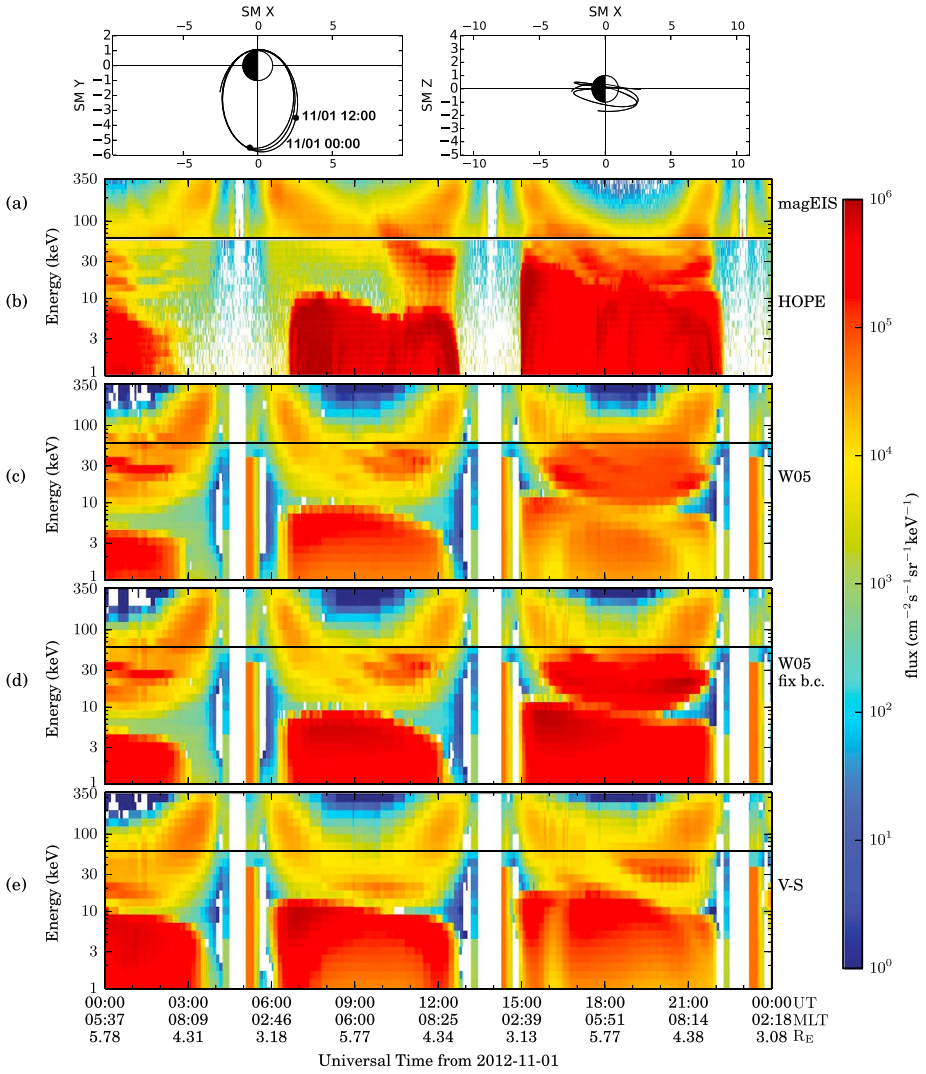

Figure 2. Observed differential H^+ flux with (a) MagEIS and (b) HOPE instruments on RBSP-B spacecraft, compared with RAM-SCB simulations driven by (c) W05 and TM03 models, (d) W05 and fixed boundary conditions, and (e) V-S and TM03 models. The horizontal black lines show the energy transition between MagEIS and HOPE. The vertical white bands indicate when the satellite is outside of the computational domain at perigee. The RBSP-B satellite orbit is plotted on top of Figure 2a for reference.

To establish prestorm conditions characteristic for the investigated period for the low-energy population on open drift paths, the simulation is run for ~8 h of quiet time before the storm commencement at ~17:00 UT (the average drift time from the nightside plasma sheet to the dayside magnetopause is ~6 h). The boundary conditions are updated every 5 min according to the MLT-dependent TM03 plasma sheet model of ion density and temperature (Figures 1c and 1d), representing the ion distribution function at 9 R_E either as Maxwellian or Kappa distribution. In this study we present results only from simulations using Kappa boundary conditions (with index $\kappa = 3$) since they showed best agreement with observations. The recent study of *Mouikis et al.* [2010] is used to correlate the ion composition at the nightside boundary with geomagnetic and solar activity.

To investigate the role of magnetospheric convection during this storm, we compare results from RAM-SCB simulations using either the solar wind-dependent W05 or the *Kp*-dependent V-S convection electric field model with observations from the Van Allen Probes. The flux at a particular spacecraft location is obtained by flying the spacecraft inside the 3-D SCB computational domain, mapping the location along the magnetic field line down to the equatorial plane, and interpolating the flux from RAM neighboring grids [*Yu et al.*, 2012]; conservation of the first and second adiabatic invariants is assumed. Comprehensive energy-time

spectrograms are thus obtained for easy comparison with Van Allen Probes data. Figure 2 shows proton fluxes for 45° pitch angle, representative of the trapped ring current population, measured on 1 November 2012, along RBSP-B orbit with MagEIS (from 50 keV to 350 keV energy) and HOPE (from 1 keV to 50 keV) instruments, compared with modeled RAM-SCB fluxes in the same energy range (note that MagEIS ion data are not available from RBSP-A for this time period). Figures 2a and 2b illustrate the high resolution, as well as excellent agreement within the continuous energy range of the ion fluxes measured with the MagEIS and HOPE instruments of the comprehensive ECT suite. The vertical white bands in the spectrograms indicate three successive perigee passes when the satellite is outside the model domain ($R_o < 2\ R_E$). The apogee traversals appear as deep reductions in the proton fluxes at high ($E > 200$ keV) energies (e.g., at ~00:00 UT, ~09:00 UT, and ~18:00 UT) since the ring current is confined closer to Earth ($R_o \leq 4.5\ R_E$).

The trapped high-energy ($E > 50$ keV) ring current population observed at radial distance $R_o < 5\ R_E$ with MagEIS is reproduced well with RAM-SCB simulations driven by either W05 or V-S models. Several dispersed ion injections (high energies appearing first due to westward drifting higher-energy ions arriving first at the spacecraft location) are observed with MagEIS (from ~100 keV) and then HOPE (down to ~20 keV) when the satellite is on the dawnside near apogee around 01:00–03:00 UT, 10:00–12:00 UT, and 16:00–18:00 UT. Similar injections are also seen in RAM-SCB simulation using W05 electric field (although not exactly at the same time); note that they are not reproduced in the simulation using the smoothly varying *Kp*-dependent V-S model (Figure 2e), which indicates that the sudden rises in the W05 field cause these particle injections.

The HOPE observations of the lower-energy ($E < 50$ keV) ring current population demonstrate the process of ring current buildup during the investigated storm period. The observed proton flux at intermediate energies from ~10 to ~40 keV remains depleted until ~11:00 UT (with the exception of some transient enhancements at large R_o at 00:00–01:00 UT) due to the loss of the preexisting trapped population and lack of fresh injections. The ring current ions in this energy range have the smallest drift velocities due to the competition of the eastward and sunward electric field drift with the westward gradient and curvature drifts and are susceptible to various loss processes (mostly charge exchange, but Coulomb collisions and plasma wave scattering could play a role). The proton flux simulated with RAM-SCB is larger than the observed flux during this time period due to either an overestimation of the initial conditions in this energy range or an underestimation of the particle losses in the expanded model (only charge exchange is considered in this first study).

The energy of the dip in the observed spectra decreases with MLT from ~12 keV at MLT = 4 at ~07:00 UT to ~6 keV at MLT = 7 at ~10:00 UT; it indicates the highest energy of the eastward drifting ions. Similar MLT dependence of the energy dip has been observed previously in dayside storm spectra [e.g., *Kistler and Larson*, 2000]. This dip refills at ~11:00 UT with newly injected ions as the convection strength increases during the storm main phase and provides easier access for these particles to the dawnside; the dip is not seen on the next satellite pass when further ion injections occur. In RAM-SCB results the stagnation dip at MLT = 6 is at ~9 keV in the simulation using W05 field in agreement with observations but at ~13 keV in the one using V-S field. These differences in the energy of the flux minima are due to the different temporal and spatial resolution of the two electric field models (Figure 1g), providing at a given time access of different energy populations to the satellite [e.g., *Kistler and Larson*, 2000]. For example, particle tracings using a V-S model with different symmetry line offsets show that a 10 keV ion with initial position at $R_o = 6.5\ R_E$ may drift eastward or westward depending on the electric field offset, thus shifting the east-west transition energy above/below 10 keV [*Jordanova et al.*, 1998]. The present study uses a standard V-S electric field with no offset. In addition, the dip does not fully refill in the simulations, indicating that the model electric field is weaker and cannot inject particles as deep as observed ($R_o \approx 4\ R_E$).

The low-energy ($E < 10$ keV) proton flux calculated with RAM-SCB intensifies during the storm main phase from ~00:00 UT to ~13:00 UT in agreement with observations. This is caused by the increased convection strength (as shown by the CPCP drop in Figure 1g) providing better access for this population and by the enhanced plasma sheet density during the first ~6 h of this period (Figure 1c). The low-energy proton flux decreases at later UT because of the simultaneous reduction of the electric field strength and the plasma sheet density. The simulations using either W05 (Figure 2c) or V-S (Figure 2e) models, however, underestimate the magnitude of the observed low-energy ($E < 10$ keV) flux after ~06 UT, the underestimation being smaller using V-S field. To highlight the importance of the plasma inflow from the magnetotail, we performed test simulations using boundary conditions with fixed ion density ($n = 0.5\ \mathrm{cm}^{-3}$) and temperature

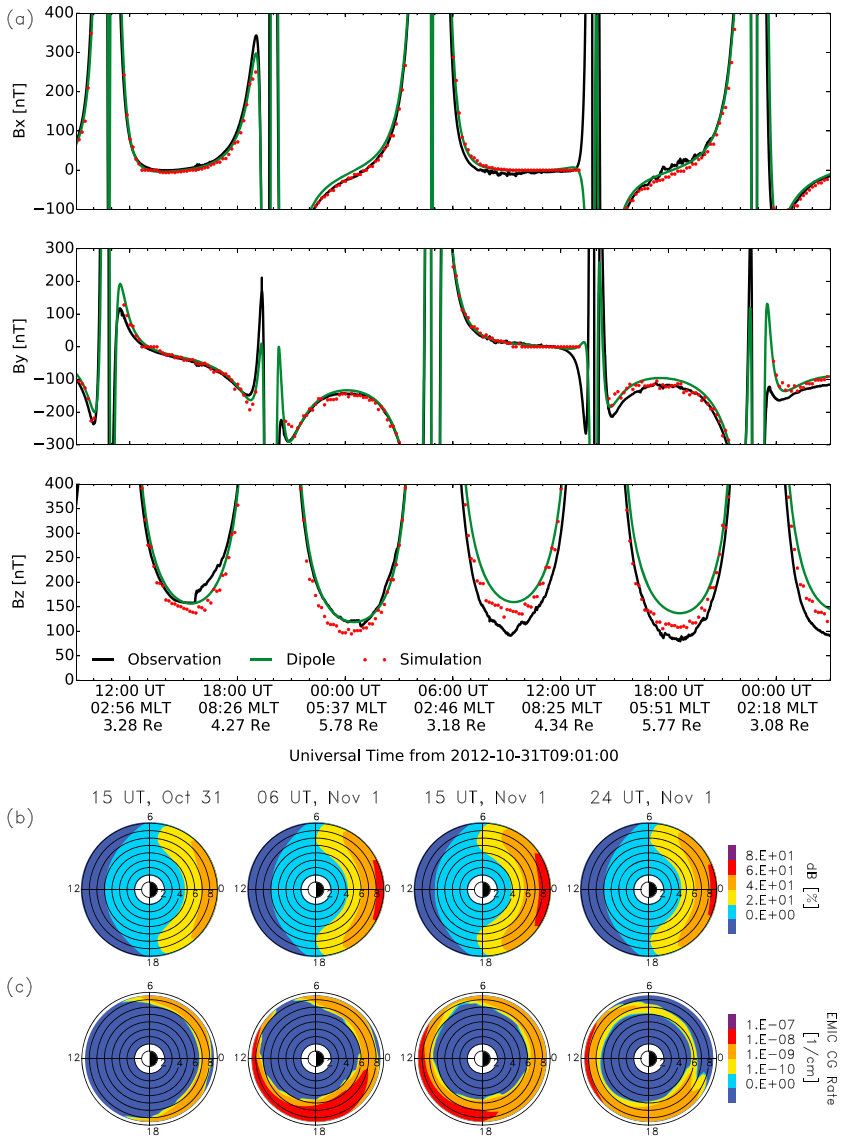

Figure 3. (a) The B_x, B_y, and B_z magnetic field components (4 s averages) in the SM coordinate system measured with EMFISIS (black line) on RBSP-B, compared with RAM-SCB simulations (dotted line) using W05 model, and with the Earth dipolar field (green line). (b) The relative difference between the intensity of the Earth dipolar field and the magnetic field calculated with RAM-SCB, and (c) the EMIC convective growth rate in the SM equatorial plane at four representative times during the storm period under investigation.

($T = 6$ keV), as shown with dashed lines in Figures 1c and 1d. The low-energy flux in this case (Figure 2d) is significantly enhanced and in better agreement with HOPE observations, indicating that the statistical TM03 model predicted too low-density and too high temperature plasma sheet population during this storm main phase. The simulated ring current O^+ and He^+ populations (not shown) exhibited similar dynamics to the ring current H^+ population and indicated that H^+ is the dominant species during this moderate storm in agreement with observations.

A distinct feature of our magnetically self-consistent ring current model is that it calculates the 3-D magnetic field in force balance with the evolving anisotropic plasma pressure of the ring current particles. RAM-SCB magnetic field calculations are compared in Figure 3 with measurements from the Electric and Magnetic Field Instrument Suite and Integrated Science (EMFISIS) investigation [*Kletzing et al.*, 2013] aboard RBSP-B. Figure 3a shows 4 s averages of the DC magnetic field vector components measured with the high-performance triaxial fluxgate EMFISIS magnetometer in the Solar Magnetic (SM) coordinate system. As discussed above, the satellite is orbiting on the dawnside with apogee at ~6 R_E and MLT ≈ 6 during this

storm period. The RAM-SCB magnetic field at a given satellite location is obtained by flying the RBSP-B satellite inside the 3-D computational domain and interpolating magnetic field values from nearby grids. Simulations using W05 model reproduce reasonably well all three components of the global magnetic field. The model predicts a significant decrease of the B_z component compared to the Earth dipolar field near apogee ($R_o > 4.5\ R_E$); however, it does not completely capture the absolute magnitude of the measured B_z. Simulation results using V-S field (not shown) are not significantly different due to the calculated similar total ion pressure.

The relative difference between the intensity of the Earth dipolar field and the self-consistently calculated RAM-SCB magnetic field in the SM equatorial plane at selected UT during the investigated period is shown in Figure 3b. Initially (15:00 UT 31 October), the magnetic field is dipolar inside of ~5 R_E. At larger distances, the magnetic field is compressed on the dayside and stronger than the dipolar field due to the magnetopause current, while it is depressed on the nightside and weaker than the dipolar field due to the tail current. As the storm develops, the decrease of the RAM-SCB field on the nightside due to the ion pressure buildup reaches ~4 R_E, indicating the need of realistic magnetic field models for accurate prediction of radiation belt dynamics during even such moderate storms. The depression becomes larger than 60% at $R_o \geq 8\ R_E$.

Figure 3c shows the generation of He^+ band EMIC waves as the storm evolves, caused by the anisotropic proton distributions obtained from RAM-SCB simulations driven with W05 model; for details on the wave growth calculations [see *Jordanova et al.*, 2010]. The convective growth rate maximizes during the storm main phase (06:00 UT 1 November) on the duskside at $R_o > 6\ R_E$, extending to ~9 R_E. This is in agreement with a recent statistical study on the global characteristics of EMIC waves from Active Magnetospheric Particle Tracer Explorers/CCE observations [*Keika et al.*, 2013]. The Van Allen Probes did not observe EMIC waves during this time as they had a dawnside orbit that did not cross the unstable region. These results demonstrate the importance of expanding the simulation domain since previous studies limited to regions inside geosynchronous orbit may have underestimated the effect of EMIC waves on the energetic particle populations. Simulated ion precipitation patterns have thus shown smaller spatial extent, confined closer to Earth, compared to Imager for Magnetopause-to-Aurora Global Exploration/FUV observations of proton arc emissions [e.g., *Jordanova et al.*, 2007].

3. Conclusions

We studied the role of convective transport and inflow of plasma from the magnetotail in the development of the ring current during the moderate storm of 1 November 2012, with our RAM-SCB model newly expanded to 9 R_E. An accurate ring current model is needed for a realistic forecast of radiation belt dynamics since the ring current population (a) represents a source population for the relativistic electrons, (b) controls the morphology of the global near-Earth magnetic field, and (c) generates plasma waves that transfer energy to the relativistic particles. Comparing simulation results with high-resolution observations from the particle and field instruments on the Van Allen Probes we found the following:

1. The expanded RAM-SCB model reproduced the initial ring current buildup caused by the simultaneous increase of the plasma sheet source population and the convective electric field. The dispersed ion injections observed with MagEIS and HOPE instruments from ~100 to ~20 keV were reproduced when the model was driven with the high-resolution W05 electric field but not with the V-S field. The observed low-energy ($E < 10$ keV) flux was underestimated by the expanded RAM-SCB during this storm main phase probably due to an underestimation of the plasma sheet density by the statistical TM03 model.
2. All three components of the large-scale magnetic field measured with EMFISIS magnetometer were reasonably well reproduced by the expanded RAM-SCB model. In agreement with observations, the calculated B_z component showed significant depression compared to the Earth dipolar field near apogee ($R_o > 4.5\ R_E$) during even this moderate storm, although it did not completely capture the magnitude of the observed depression.
3. The expanded RAM-SCB model revealed a larger region on the duskside (from ~6 to ~9 R_E) where the growth rate of He^+ band EMIC waves intensified during the storm main phase, suggesting that previous models having geosynchronous orbit as an outer boundary have underestimated the scattering effect from these waves on the ring current ions and radiation belt electrons.

Acknowledgments
This work was supported by JHU/APL contracts 967399 and 921647 under NASA prime contract NAS5-01072. The work at LANL was conducted under the auspices of the U.S. Department of Energy, with partial support from the NASA LWS and NSF GEM programs. We thank the OMNIWeb from NASA Goddard Space Flight Center for providing the solar wind observation data and the geomagnetic indices.

The Editor thanks two anonymous reviewers for their assistance in evaluating this paper.

References

Blake, J. B., et al. (2013), The magnetic electron ion spectrometer (MagEIS) instruments aboard the radiation belt storm probes (RBSP) spacecraft, *Space Sci. Rev.*, *179*, 383–421, doi:10.1007/s11214-013-9991-8.

Chappell, C. R., T. E. Moore, and J. H. Waite Jr. (1987), The ionosphere as a fully adequate source of plasma for the Earth's magnetosphere, *J. Geophys. Res.*, *92*, 5896–5910, doi:10.1029/JA092iA06p05896.

Daglis, I. A., E. T. Sarris, and B. Wilken (1993), AMPTE/CCE CHEM observations of the energetic ion population at geosynchronous altitudes, *Ann. Geophys.*, *11*, 685–696.

Funsten, H., et al. (2013), Helium, oxygen, proton, and electron (HOPE) mass spectrometer for the Radiation Belt Storm Probes mission, *Space Sci. Rev.*, *179*, 423–484, doi:10.1007/s11214-013-9968-7.

Jordanova, V. K. (2012), The role of the Earth's ring current in radiation belt dynamics, in *Dynamics of the Earth's Radiation Belts and Inner Magnetosphere, Geophys. Monogr. Ser.*, vol. 199, edited by D. Summers et al., pp. 303–313, AGU, Washington, D. C., doi:10.1029/2012GM001330.

Jordanova, V. K., et al. (1998), October 1995 magnetic cloud and accompanying storm activity: Ring current evolution, *J. Geophys. Res.*, *103*, 79–92, doi:10.1029/97JA02367.

Jordanova, V. K., M. Spasojevic, and M. F. Thomsen (2007), Modeling the EMIC wave-induced formation of detached subauroral proton arcs, *J. Geophys. Res.*, *112*, A08209, doi:10.1029/2006JA012215.

Jordanova, V. K., S. Zaharia, and D. T. Welling (2010), Comparative study of ring current development using empirical, dipolar, and self-consistent magnetic field simulations, *J. Geophys. Res.*, *115*, A00J11, doi:10.1029/2010JA015671.

Keika, K., K. Takahashi, A. Y. Ukhorskiy, and Y. Miyoshi (2013), Global characteristics of electromagnetic ion cyclotron waves: Occurrence rate and its storm dependence, *J. Geophys. Res. Space Physics*, *118*, 4135–4150, doi:10.1002/jgra.50385.

Kim, H.-J., and A. A. Chan (1997), Fully adiabatic changes in storm time relativistic electron fluxes, *J. Geophys. Res.*, *102*, 22,107–22,116.

Kistler, L. M., and D. J. Larson (2000), Testing electric and magnetic field models of the storm-time inner magnetosphere, *J. Geophys. Res.*, *105*, 25,221–25,231, doi:10.1029/2000JA000132.

Kletzing, C. A., et al. (2013), The Electric and Magnetic Field Instrument Suite and Integrated Science (EMFISIS) on RBSP, *Space Sci. Rev.*, *179*, 127–181, doi:10.1007/s11214-013-9993-6.

Le, G., C. T. Russell, and K. Takahashi (2004), Morphology of the ring current derived from magnetic field observations, *Ann. Geophys.*, *22*, 1267–1295.

Lemon, C., R. A. Wolf, T. W. Hill, S. Sazykin, R. W. Spiro, F. R. Toffoletto, J. Birn, and M. Hesse (2004), Magnetic storm ring current injection modeled with the Rice Convection Model and a self-consistent magnetic field, *Geophys. Res. Lett.*, *31*, L21801, doi:10.1029/2004GL020914.

Mauk, B. H., N. J. Fox, S. G. Kanekal, R. L. Kessel, D. G. Sibeck, and A. Ukhorskiy (2012), Science objectives and rationale for the Radiation Belt Storm Probes Mission, *Space Sci. Rev.*, *179*, 3–27, doi:10.1007/s11214-012-9908-y.

Mouikis, C. G., L. M. Kistler, Y. H. Liu, B. Klecker, A. Korth, and I. Dandouras (2010), H^+ and O^+ content of the plasma sheet at 15–19 Re as a function of geomagnetic and solar activity, *J. Geophys. Res.*, *115*, A00J16, doi:10.1029/2010JA015978.

Powell, K. G., P. L. Roe, T. J. Linde, T. I. Gombosi, and D. L. De Zeeuw (1999), A solution-adaptive upwind scheme for ideal magnetohydrodynamics, *J. Comp. Phys.*, *154*, 284–309.

Spence, H. E., et al. (2013), Science goals and overview of the Radiation Belt Storm Probes (RBSP) energetic particle, composition, and thermal plasma (ECT) suite on NASA's Van Allen Probes Mission, *Space Sci. Rev.*, *179*, 311–336, doi:10.1007/s11214-013-0007-5.

Stern, D. P. (1975), The motion of a proton in the equatorial magnetosphere, *J. Geophys. Res.*, *80*, 595–599, doi:10.1029/JA080i004p00595.

Summers, D., R. M. Thorne, and F. Xiao (1998), Relativistic theory of wave-particle resonant diffusion with application to electron acceleration in the magnetosphere, *J. Geophys. Res.*, *103*, 20,487–20,500, doi:10.1029/98JA01740.

Thorne, R. M., R. B. Horne, V. K. Jordanova, J. Bortnik, and S. A. Glauert (2006), Interaction of EMIC waves with thermal plasma and radiation belt particles, in *Magnetospheric ULF Waves: Synthesis and New Directions, Geophys. Monogr. Ser.*, vol. 169, pp. 213–223, AGU, Washington, D. C.

Troshichev, O. A., V. G. Andrezen, S. Vennerstrøm, and E. Friis-Christensen (1988), Magnetic activity in the Polar Cap: A new index, *Planet. Space Sci.*, *36*, 1095–1102.

Tsyganenko, N. A. (1989), A magnetospheric magnetic field model with a warped tail current sheet, *Planet. Space Sci.*, *37*, 5–20.

Tsyganenko, N. A., and T. Mukai (2003), Tail plasma sheet models derived from geotail particle data, *J. Geophys. Res.*, *108*, 1136, doi:10.1029/2002JA009707.

Volland, H. (1973), A semiempirical model of large-scale magnetospheric electric fields, *J. Geophys. Res.*, *78*, 171–180, doi:10.1029/JA078i001p00171.

Weimer, D. R. (2005), Improved ionospheric electrodynamic models and application to calculating Joule heating rates, *J. Geophys. Res.*, *110*, A05306, doi:10.1029/2004JA010884.

Yu, Y., V. Jordanova, S. Zaharia, J. Koller, J. Zhang, and L. M. Kistler (2012), Validation study of the magnetically self-consistent inner magnetosphere model RAM-SCB, *J. Geophys. Res.*, *117*, A03222, doi:10.1029/2011JA017321.

Zaharia, S., V. K. Jordanova, M. F. Thomsen, and G. D. Reeves (2006), Self-consistent modeling of magnetic fields and plasmas in the inner magnetosphere: Application to a geomagnetic storm, *J. Geophys. Res.*, *111*, A11S14, doi:10.1029/2006JA011619.